Repurposing erectile dysfunction drugs tadalafil and vardenafil to increase bone mass

Se-Min Kim[a,b,1], Charit Taneja[a,b], Helena Perez-Pena[c], Vitaly Ryu[a,b], Anisa Gumerova[a,b], Wenliang Li[c], Naseer Ahmad[a,b], Ling-Ling Zhu[a,b], Peng Liu[a,b], Mehr Mathew[a,b], Funda Korkmaz[a,b], Sakshi Gera[a,b], Damini Sant[a,b], Elina Hadelia[a,b], Kseniia Ievleva[a,b,d], Tan-Chun Kuo[a,b], Hirotaka Miyashita[a,b], Li Liu[e,f], Irina Tourkova[e,f], Sarah Stanley[b], Daria Lizneva[a,b], Jameel Iqbal[a,b], Li Sun[a,b], Ronald Tamler[b], Harry C. Blair[e,f], Maria I. New[a,g,1], Shozeb Haider[c], Tony Yuen[a,b,2], and Mone Zaidi[a,b,2]

[a]The Mount Sinai Bone Program, Icahn School of Medicine at Mount Sinai, New York, NY 10029; [b]Department of Medicine, Icahn School of Medicine at Mount Sinai, New York, NY 10029; [c]Department of Pharmaceutical and Biological Chemistry, University College London School of Pharmacy, WC1N 1AX London, United Kingdom; [d]Department of Reproductive Health, Scientific Center for Family Health and Human Reproduction Problems, 664003 Irkutsk, Russian Federation; [e]Department of Pathology, Pittsburgh Veterans Affairs Healthcare System, Pittsburgh, PA 15240; [f]Department of Pathology, University of Pittsburgh, Pittsburgh, PA 15261; and [g]Department of Pediatrics, Icahn School of Medicine at Mount Sinai, New York, NY 10029

Contributed by Maria I. New, April 17, 2020 (sent for review January 27, 2020; reviewed by Yousef Abu-Amer, Fayez F. Safadi, and Mei Wan)

We report that two widely-used drugs for erectile dysfunction, tadalafil and vardenafil, trigger bone gain in mice through a combination of anabolic and antiresorptive actions on the skeleton. Both drugs were found to enhance osteoblastic bone formation in vivo using a unique gene footprint and to inhibit osteoclast formation. The target enzyme, phosphodiesterase 5A (PDE5A), was found to be expressed in mouse and human bone as well as in specific brain regions, namely the locus coeruleus, raphe pallidus, and paraventricular nucleus of the hypothalamus. Localization of PDE5A in sympathetic neurons was confirmed by coimmunolabeling with dopamine β-hydroxylase, as well as by retrograde bone-brain tracing using a sympathetic nerve-specific pseudorabies virus, PRV152. Both drugs elicited an antianabolic sympathetic imprint in osteoblasts, but with net bone gain. Unlike in humans, in whom vardenafil is more potent than tadalafil, the relative potencies were reversed with respect to their osteoprotective actions in mice. Structural modeling revealed a higher binding energy of tadalafil to mouse PDE5A compared with vardenafil, due to steric clashes of vardenafil with a single methionine residue at position 806 in mouse PDE5A. Collectively, our findings suggest that a balance between peripheral and central actions of PDE5A inhibitors on bone formation together with their antiresorptive actions specify the osteoprotective action of PDE5A blockade.

osteoporosis | resorption | cyclic GMP | PDE5 inhibitor | computational modeling

Since the initial description of the effects of nitric oxide (NO) on bone cells (1), physiological studies over two decades have confirmed its critical role in skeletal homeostasis. Notably, NO and its donors suppress the activity of the osteoclast, the cell that resorbs bone, and also stimulate bone formation by osteoblasts (1–7). Osteoclasts also generate NO in the local resorptive microenvironment (7), and mice lacking NO synthase display an osteoporotic phenotype (8). The therapeutic potential for long-term NO donor therapy, such as nitroglycerin, sodium nitroprusside, and nitrosyl-cobinamide, for osteoporosis has also been explored (4, 9–13). Individuals receiving NO donor therapy display higher hip bone mineral density (BMD) and a reduced risk of fracture (14, 15). Nonetheless, chronic NO-based therapy is currently restricted for use in conditions of vascular dysfunction, such as recurrent angina and pulmonary hypertension (16, 17).

The downstream target of NO is soluble guanylate cyclase-cyclic guanosine monophosphate (cGMP)–dependent protein kinase G (PKG). PKG is a serine-threonine protein kinase that is inactivated by family of specific cGMP-degrading phosphodiesterases (PDEs). Gain and loss of function of PKG in murine models, namely in $Prkg2^{R242Q}$ and $Prkg2^{-/-}$ mice, result in increases and decreases in bone mass, respectively (18, 19). Likewise, soluble guanylate cyclase has also been targeted for bone gain (20, 21). Overall, the results to date establish a primary role for the NO-cGMP-PKG axis in skeletal regulation, and suggest that the inhibition of PDEs could offer osteoprotection by activating PKG.

Of the 11 PDEs present in mammalian tissues (22), PDE5A is the inhibitory target for the three widely used drugs for erectile dysfunction: namely sildenafil, tadalafil, and vardenafil. Pharmacologic studies using recombinant PDE5A show that vardenafil is 10-fold more potent than tadalafil in inhibiting the human enzyme (22). Of note, 70% of men age >70 y who have experienced erectile dysfunction are potential candidates for PDE5A inhibitor therapy (23). In fact, following the release of the first PDE5 inhibitor, sildenafil, in 1998, the rate of PDE5A inhibitor use in the Veterans Health Administration grew to 105 per 1,000 male patients (24). With the availability of generic forms of these drugs, their use is likely to accelerate in an increasingly aged male population.

Significance

Tadalafil and vardenafil are among the most widely used drugs for erectile dysfunction, which affects nearly 19% of men over 20 y of age. Older men also suffer from age-related bone loss resulting in crippling fractures. We show that in mice, both agents act on bone cells, resulting in the formation of new bone and reduced removal of old bone. Because of this net gain in bone mass, we posit that tadalafil and vardenafil could be used for cotreating erectile dysfunction and osteoporosis in men of advancing age, as well as for treating osteoporosis in postmenopausal women. We recommend future clinical studies to establish the capability of these drugs to increase bone density and reduce fracture risk in humans.

Author contributions: S.-M.K., R.T., H.C.B., M.I.N., S.H., T.Y., and M.Z. designed research; S.-M.K., C.T., H.P.-P., V.R., A.G., W.L., N.A., L.-L.Z., P.L., F.K., D.S., E.H., K.I., T.-C.K., L.L., I.T., and L.S. performed research; S.S. contributed new reagents/analytic tools; S.-M.K., C.T., H.P.-P., V.R., A.G., W.L., L.-L.Z., M.M., S.G., E.H., H.M., L.L., I.T., D.L., J.I., L.S., H.C.B., S.H., T.Y., and M.Z. analyzed data; and S.-M.K., M.I.N., T.Y., and M.Z. wrote the paper.

Reviewers: Y.A., Washington University Medical Center; F.F.S., Northeast Ohio Medical University; and M.W., Johns Hopkins University School of Medicine.

The authors declare no competing interest.

[1]To whom correspondence may be addressed. Email: se-min.kim@mountsinai.org or maria.new@mssm.edu.

[2]T.Y. and M.Z. contributed equally to this work.

This article contains supporting information online at https://www.pnas.org/lookup/suppl/doi:10.1073/pnas.2000950117/-/DCSupplemental.

First published June 8, 2020.

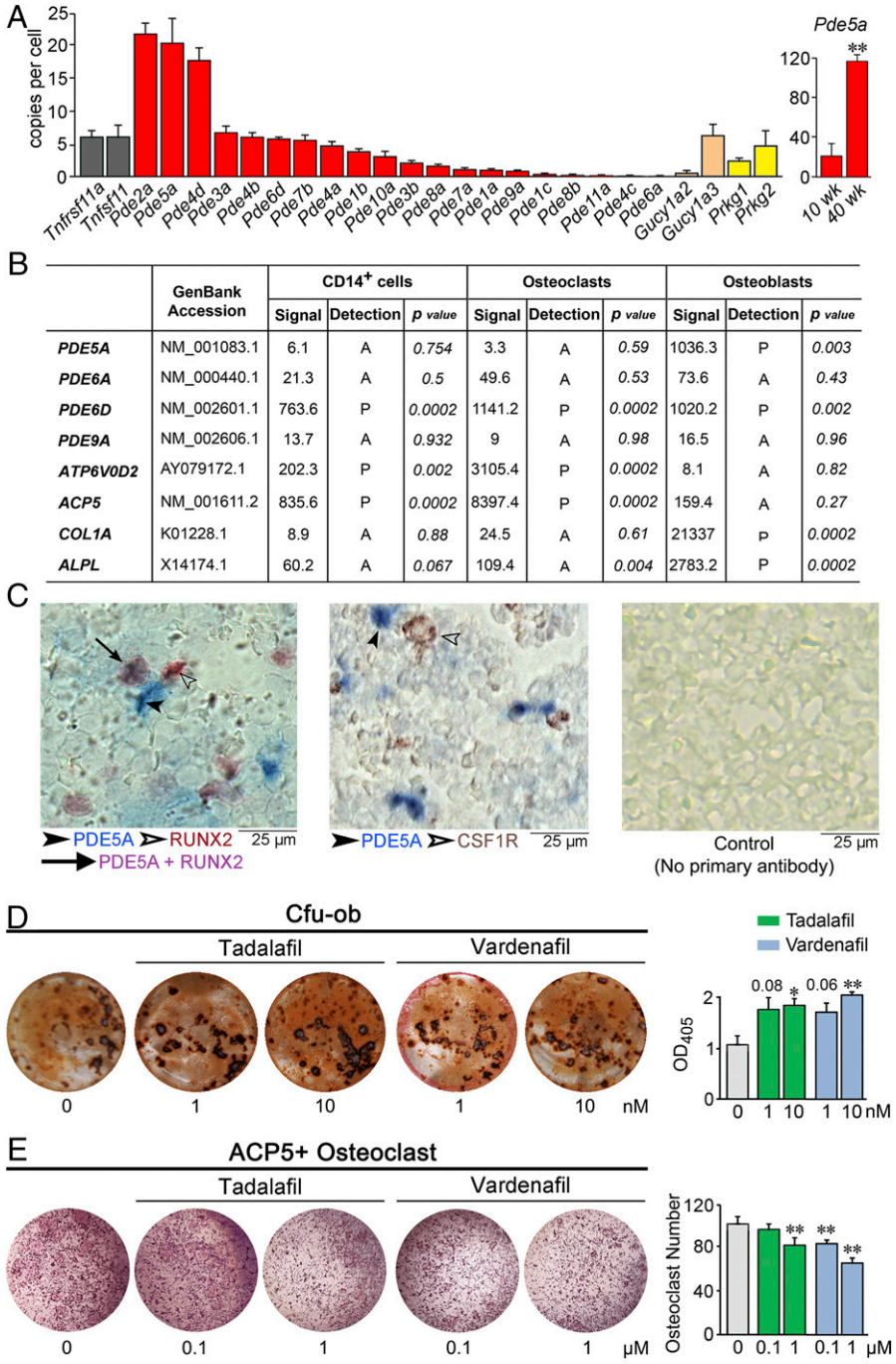

	GenBank Accession	CD14+ cells			Osteoclasts			Osteoblasts		
		Signal	Detection	*p value*	Signal	Detection	*p value*	Signal	Detection	*p value*
PDE5A	NM_001083.1	6.1	A	*0.754*	3.3	A	*0.59*	1036.3	P	*0.003*
PDE6A	NM_000440.1	21.3	A	*0.5*	49.6	A	*0.53*	73.6	A	*0.43*
PDE6D	NM_002601.1	763.6	P	*0.0002*	1141.2	P	*0.0002*	1020.2	P	*0.002*
PDE9A	NM_002606.1	13.7	A	*0.932*	9	A	*0.98*	16.5	A	*0.96*
ATP6V0D2	AY079172.1	202.3	P	*0.002*	3105.4	P	*0.0002*	8.1	A	*0.82*
ACP5	NM_001611.2	835.6	P	*0.0002*	8397.4	P	*0.0002*	159.4	A	*0.27*
COL1A	K01228.1	8.9	A	*0.88*	24.5	A	*0.61*	21337	P	*0.0002*
ALPL	X14174.1	60.2	A	*0.067*	109.4	A	*0.004*	2783.2	P	*0.0002*

Fig. 1. Expression and in vitro actions of PDE5A inhibitors tadalafil and vardenafil. (*A*) TaqMan-based PCR using bone RNA showing the expression of 20 murine PDE isoforms, soluble guanylate cyclase isoforms (*Gucy1a2* and *Gucy1a3*), protein kinase G isoforms (*Prkg1* and *Prkg2*), as well as *Tnfrsf11a* and *Tnfsf11* (controls). SYBR Green-based PCR using bone RNA from 10- and 40-wk-old mice showing the expression of *Pde5a*. Data are expressed as copy number per cell (normalized to *Tubulin*, *Rps11*, *Actb*, and/or *Gapdh*). Data are mean ± SEM. $n = 3$ biological replicates for TaqMan; $n = 4$ biological replicates for SYBR Green. (*B*) Data obtained from Human Genome U133 2.0 GeneChip Arrays (Affymetrix). The presence of transcripts was determined from the signal of perfect matched and mismatched probe pairs in each probe set, with statistical confidence (*P* value) indicated. Characteristic highly expressed osteoclastic and osteoblastic transcripts are also included as controls. (*C*) Photomicrographs showing immune labeling of PDE5A (blue, solid arrowhead) and RUNX2 (*Left*) or CSF1R (*Middle*) (brown, hollow arrowhead) in mouse bone marrow (colocalization is shown in purple, solid arrow), together with a control image without primary antibody (*Right*) (details in *Methods*). (*D*) Effect of tadalafil and vardenafil on Cfu-ob in 21-d cultures of bone marrow stromal cells isolated from marrow of 10-mo-old male mice in differentiating medium, shown as representative alizarin red-positive Cfu-ob and mean ± SEM absorbance of extracted dye per well (in triplicate). (*E*) Effect of tadalafil and vardenafil on tartrate-resistant acid phosphatase-positive ($ACP5^+$) osteoclasts at 5 d following the incubation of bone marrow hematopoietic stem cells with RANKL and M-CSF, shown as representative plates and mean ± SEM $ACP5^+$ osteoclast number per well (in triplicate). Statistics for *D* and *E*: unpaired two-tailed Student's *t* test; $*P < 0.05$, $**P < 0.01$, or as shown.

The relatively ubiquitous expression of PDEs has prompted a careful examination of the extragenital actions of PDE5A inhibition. For example, tadalafil and vardenafil have been used for pulmonary hypertension (25). Likewise, PDE5A is expressed in the brain, and its inhibition affects neurogenesis, memory, and stroke progression (26–28). PDE5A is also expressed in chondrocytes, but inhibiting PDE5A in 1-mo-old rats for 3 wk did not affect long bone growth or bone modeling (29). Other studies on putative skeletal effects of PDE5A inhibition in animal models have yielded inconsistent results, including hyperresorption and low bone density (30), positive effects on bone in ovariectomized and glucocorticoid-treated mice (31, 32), and accelerated fracture healing (33).

Here we report a comprehensive analysis of the effects of PDE5A inhibition on bone formation, bone resorption, and bone mass. We also evaluate the contribution of central actions mediated via PDE5A-containing neurons in the brain. We find that tadalafil and vardenafil increase bone mass through combined actions on osteoblasts and osteoclasts, as well as on hippocampal neurons. This net positive effect on bone mass could be therapeutically meaningful to protect against bone loss in men age >50 y, 47% of whom have osteopenia (34).

Results

We first carried out unbiased TaqMan-based expression profiling of 20 murine PDE isoforms using whole-bone RNA (Fig. 1*A*). Three PDEs—*Pde2a*, *5a*, and *4d*—were expressed at high levels (>15 copies per cell) compared with *Tnfrsf11a* and *Tnfsf11*, which encode for RANK and RANKL, respectively (Fig. 1*A*). Of note, *Pde5a* expression in 40-wk-old mice was significantly greater than that in young mice, suggesting that PDE5A could be targeted in older individuals to prevent bone loss. Furthermore, other molecular components of the NO-cGMP-PKG axis, including soluble guanylate cyclase (*Gucy1a2* and *Gucy1a3)* and protein kinase G (*Prkg1* and *Prkg2*) isoforms, were also expressed in bone. Previous studies with bovine tissue have documented high *Pde2a* expression in the adrenal gland, kidney, heart, and hippocampus (35). PDE2A binds cGMP at physiological concentrations to induce a conformational change that enhances its affinity for 3′,5′-cyclic adenosine monophosphate (cAMP). Although at higher concentrations, it competes to hydrolyze cGMP preferentially, PDE2A is not a target for tadalafil or vardenafil, which exhibit IC_{50} values >10,000 fold higher than those for PDE5A (22). Unlike PDE2A, PDE4D hydrolyzes cAMP, but not cGMP, and is again not a known target for tadalafil or vardenafil.

Fig. 1*B* shows Affymetrix microarray data using cultured human $CD14^+$ hematopoietic stem cell precursors, osteoclasts, and osteoblasts. Of note, genes encoding for the corresponding human PDE isoforms, namely *PDE5A* and *PDE6D*, were expressed in osteoblasts (Fig. 1*B*). In addition, *PDE6D* was expressed in $CD14^+$ cells as well as osteoclasts (Fig. 1*B*). However, PDE6D is a noncatalytic PDE subunit and thus is not a target for tadalafil or vardenafil. *PDE6A* and *PDE9A* were not expressed in human bone cells, consistent with their very low expression in mouse bone (Fig. 1 *A* and *B*). The osteoclast-specific genes *ATP6V0D2* and *ACP5*, as well as osteoblast-specific genes *COL1A1* and *ALPL*, were expressed in the two cell types, confirming cellular identity. Fig. 1*C* shows the colocalization (purple) of PDE5A immunoreactivity (blue) with RUNX2 (brown) in murine bone marrow stromal cells, confirming the localization of PDE5A protein in osteoblast precursors. No such costaining of $PDE5A^+$ and $CSF1R^+$ cells was noted, suggesting the absence of the enzyme in osteoclasts.

Therefore, we examined the effects of tadalafil and vardenafil on the formation of mineralizing osteoblasts from these precursors. To study osteoblastogenesis in vitro, we cultured murine bone marrow stromal cells in differentiating medium in the presence of tadalafil or vardenafil for 21 d. A significant increase in colony formation, colony-forming units–osteoblastoids (Cfu-ob), was noted with tadalafil and vardenafil (Fig. 1*D*). In parallel, both drugs reduced tartrate-resistant acid phosphatase (ACP5)-positive osteoclasts formed when hematopoietic stem cells were cultured for 5 d in the presence of RANK-L and macrophage colony-stimulating factor (M-CSF) (Fig. 1*E*). Together, these studies document both pro-osteoblastic and antiosteoclastic actions of the two agents.

Increases in bone mass can arise from cell-autonomous actions of a molecule on bone cells—osteoblasts, best illustrated by the anabolic actions of parathyroid hormone (36), or osteoclasts, as with calcitonin (37). Central neural circuits converging on sympathetic and parasympathetic relays at the level of the osteoblast also affect bone mass (38–40). Sympathetic relay in particular exerts an antianabolic action by reducing osteoblast proliferation, and drugs such as propranolol show positive actions on bone mass and reduced fracture risk (41, 42). Thus, the overall effects on bone mass are a composite of anabolic and antianabolic actions on osteoblasts along with the modulation of osteoclastic bone resorption.

Given that PDE5A is expressed in the brain with multiple predicted neural actions (26–28), we sought to explore whether PDE5A inhibition has a role in bone mass regulation via the well-characterized sympathetic innervation of bone (39). Confocal immunofluorescence imaging of brain tissue from wild-type C57BL/6 mice showed PDE5A labeling in the locus coeruleus, raphe pallidus, and paraventricular nucleus of the hypothalamus (Fig. 2*A* and *SI Appendix*, Fig. S1 *A* and *B*). A subpopulation of $PDE5A^+$ neurons exhibited immunoreactivity for dopamine β-hydroxylase (DBH), suggesting that multiple distributed nodes of the sympathetic nervous system could be modulated by PDE5A (Fig. 2*A*).

To further examine whether these PDE5A/DBH double-labeled neurons project into bone, we used a transsynaptic tracing technique with a pseudorabies virus strain, PRV152. PRV152 expresses enhanced green fluorescent protein (EGFP) under control of the human cytomegalovirus immediate-early promoter. When injected into peripheral tissues, the virus travels exclusively in a retrograde manner and localizes to central neurons (Fig. 2*B*); thus, it has been used widely for tracing tissue–neuronal connections (43). Injection of PRV152 under the bone periosteum or into metaphyseal bone, areas of abundant sympathetic innervation, resulted in detection of EGFP in the PDE5A-rich areas noted above at 6 d following injection in anesthetized mice (Fig. 2*B*). No EGFP signal was detected when PRV152 was placed on the bone surface rather than injected under the periosteum or into metaphyseal bone (*SI Appendix*, Fig. S1 *C* and *D*). Collectively, the foregoing data establish a direct anatomic connection between PDE5A-containing neurons in specific brain areas and bone, raising the possibility of a contribution of this central axis to the bone-forming actions of PDE5A inhibitors.

To evaluate the effect of PDE5 inhibition on bone mass and microarchitecture in vivo, we used 14-wk-old female C57BL/6 mice. Areal BMD was evaluated by dual energy X-ray absorptiometry (DXA; PIXimus; GE Healthcare) at baseline and then every 2 wk following oral gavage with vehicle, tadalafil (2 mg/kg/d), or vardenafil (10 mg/kg/d). In vehicle-treated mice, areal BMD increased over 6 wk, while tadalafil- and vardenafil-treated mice displayed greater increases in BMD, with the effect of tadalafil reaching statistical significance compared with vehicle (Fig. 3*A*). There were also variations in BMD gain at the different sites (Fig. 3*A*).

To replicate the areal BMD data, we euthanized the mice after 6 wk of treatment. The vertebral column was dissected and processed for microcomputed tomography (μ-CT) to assess structural parameters. Consistent with representative images (shown), volumetric BMD (vBMD) and fractional bone volume (BV/TV) were increased significantly or showed trends toward significance with tadalafil and vardenafil, respectively. The somewhat larger response

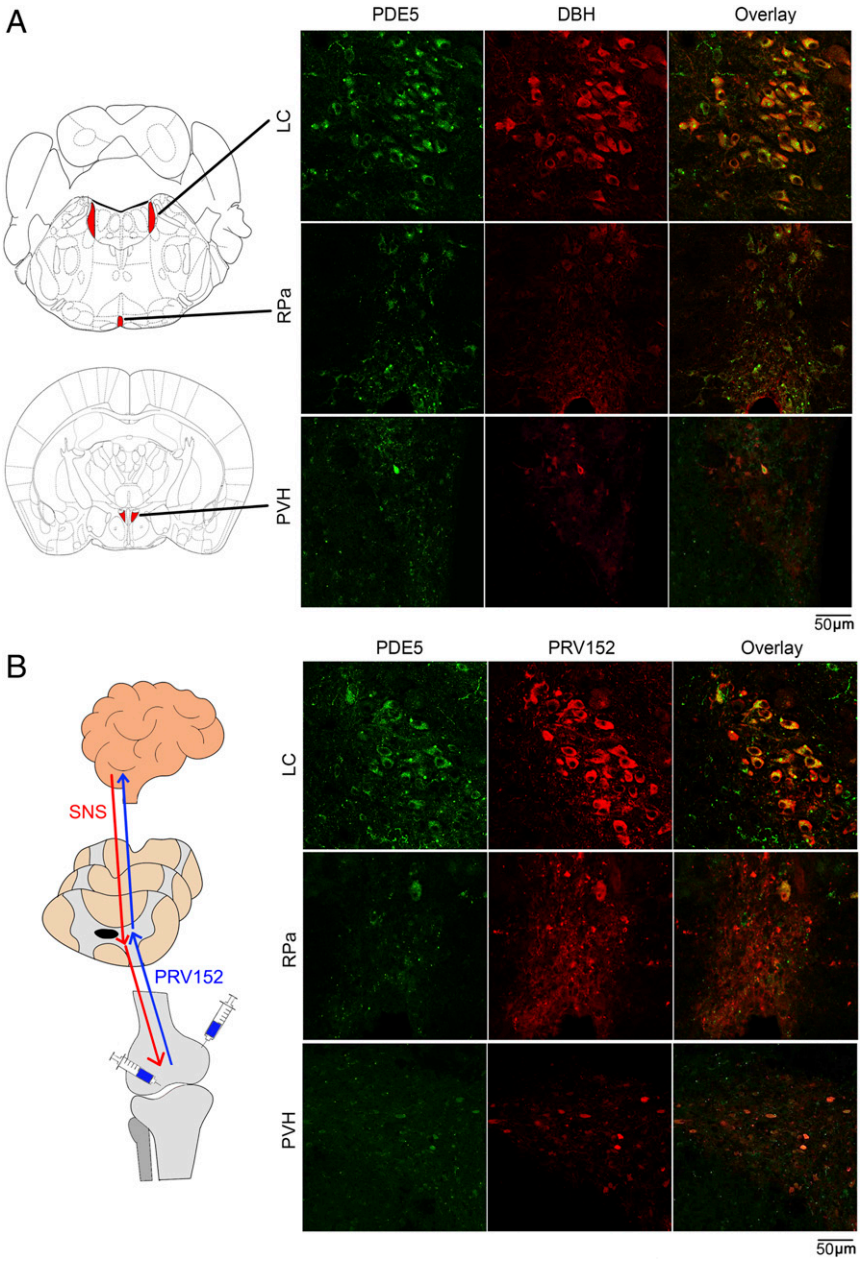

Fig. 2. Localization of PDE5A in sympathetic neurons in three brain regions. (*A*) Representative confocal photomicrographs showing the colocalization (yellow) of PDE5A (green) and DBH (red) immunolabeling in a number of neurons of the locus coeruleus (LC), raphe pallidus (RPa), and paraventricular nucleus of the hypothalamus (PVH). Also shown is the map of brain areas. (*B*) Retrograde transsynaptic virus-mediated tract tracing using a pseudorabies virus strain, PRV152, that expresses EGFP under control of the human cytomegalovirus immediate-early promoter. PRV152 was injected into the metaphysis or subperiosteally (shown as schematic) in live anesthetized mice at 6 d before sacrifice. Brain regions were dissected and processed for PDE5A (green) and EGFP (red) immunohistochemistry. The virus traversed from bone via the sympathetic nervous system to the three brain regions, LC, Rpa, and PVH, where it colocalized with PDE5A (yellow). Refer to *SI Appendix*, Fig. S1.

magnitude with tadalafil was consistent with the areal BMD data (Fig. 3 *A* and *B*). Trabecular number (Tb.N) tended to be higher with corresponding decrements in trabecular spacing (Tb.Sp), while there was no effect on trabecular thickness (Tb.Th). Based on the collective DXA and μ-CT data, tadalafil displayed more robust increases in bone mass compared with vardenafil.

To achieve further granularity of the bone mass effect, we examined the effects of the two drugs on bone formation and resorption. For bone formation parameters, dynamic histomorphometry was performed on the vertebral column after 6 wk of drug treatment and following the injection of calcein (15 mg/kg) at days –7 and –2 before euthanasia (Fig. 4*A*). The figure shows fluorescent labels indicative of new bone formation with magnification of selected areas, together with quantitative analysis of sections from mice for each group (Fig. 4 *A* and *B*). Both tadalafil and vardenafil significantly increased the mineralizing surface (MS), mineral apposition rate (MAR), and bone formation rate (BFR) (Fig. 4*B*). To explore the effects of PDE5A inhibition on bone resorption, we examined the number of osteoclasts labeled for ACP5 (tartrate-resistant acid phosphatase), shown in the photomicrographs (Fig. 4*A*). Both tadalafil and vardenafil reduced ACP5-positive osteoclast number

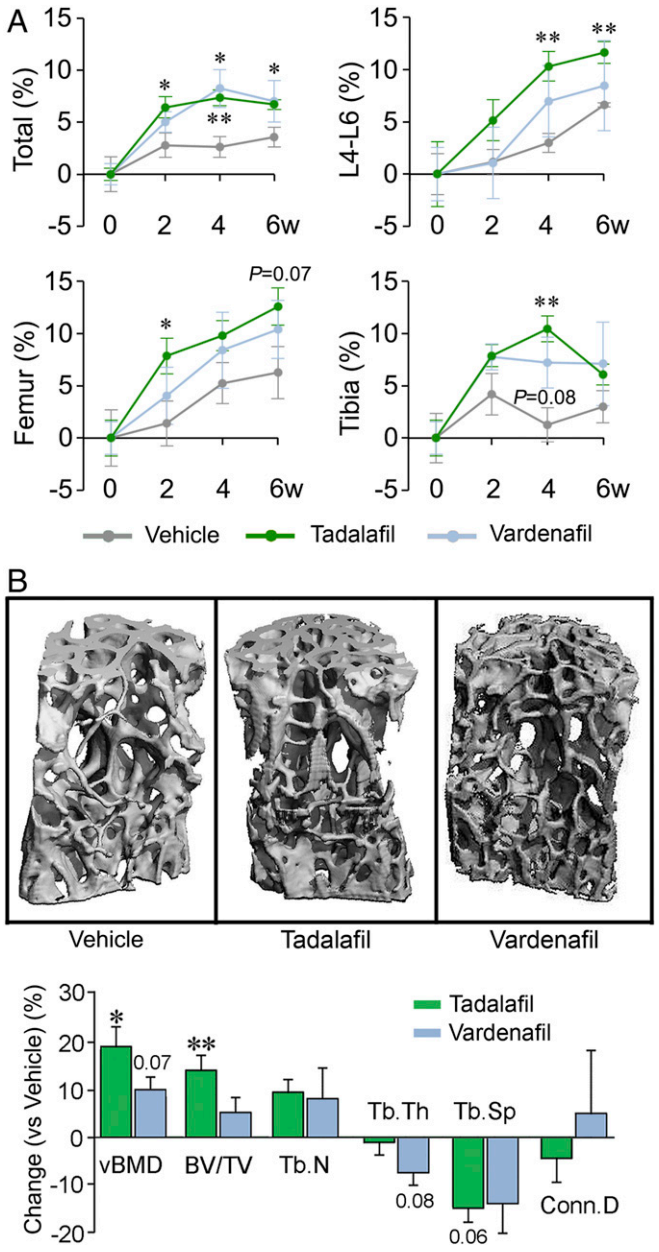

Fig. 3. PDE5A inhibitors tadalafil and vardenafil increase bone mass. (*A*) Areal BMD of the total skeleton and of L4-6 vertebrae and right femur and tibia in female mice treated with vehicle (gray), tadalafil (green), or vardenafil (blue) measured at 0, 2, 4, and 6 wk by a PIXimus small animal densitometer (details and doses in *Methods*). (*B*) Representative images of 3D reconstructions of L5 vertebral trabecular bone at 6 wk following vehicle or drug treatment. Static quantitative morphometry from μ-CT, providing measures of vBMD, BV/TV, Tb.N, Tb.Th, Tb.Sp, and connectivity density (Conn.D). Data are shown as mean percent change ± SEM (vs. vehicle). Statistics: two-tailed Student's *t* test; $*P < 0.05$, $**P < 0.01$, or as shown vs. vehicle; $n = 4$ to 5 mice per group.

expressed per bone surface or bone volume (Fig. 4*C*); this is consistent with an action of both drugs on osteoclast formation noted in vitro (cf. Fig. 1*E*).

For the PDE5A inhibitor-induced anabolic actions, we sought to dissect direct actions of the respective drugs on osteoblasts vs. potential indirect effects exerted via sympathetic relay. Tadalafil and vardenafil yielded matched gene signatures in terms of up-regulated and down-regulated osteoblastogenic genes in bone marrow stromal cells following in vivo exposure (Fig. 4 *D* and *E*). Namely, *Ogn* and *Bsp* were up-regulated by both drugs, consistent with an anabolic action, whereas *Bmp2* was down-regulated (Fig. 4 *D* and *E*). The expression levels of *Alp*, *Runx2*, *Tnfsf11*, and *Col1a1* remained relatively unchanged with both drugs. We also examined the expression of protein kinase G isoforms, of which PKG2 is a downstream target of PDE5A. *Prkg2* was up-regulated significantly in osteoblast precursors derived from tadalafil-treated mice, with a trend toward significance ($P = 0.08$) in vardenafil-exposed cells (Fig. 4*F*). The expression of *Prkg1*, which is not a PDE5A target, was unaffected by either drug.

Because centrally located PDE5A-positive sympathetic neurons were found to innervate bone (Fig. 2), we also studied the well-characterized "sympathetic bone" gene signature (39, 44), consisting mainly of clock genes, in osteoblast precursors from tadalafil- and vardenafil-treated mice. This latter footprint is known to modulate precursor proliferation, rather than differentiation (39, 44). Both tadalafil and vardenafil suppressed this gene signature with the down-regulation of *Per1*, *Per2*, and *Bmal1*, as well as of *Myc* and *Ccnd* (Fig. 4*G*). Such a reduction in genes known to be regulated by sympathetic discharge, prominently cyclin D, would be consistent with reduced proliferation of osteoblast precursors. In parallel, the direct anabolic actions of PDE5A inhibition on this pool of precursors would induce their differentiation into mature mineralizing osteoblasts (cf. Fig. 1*D*). Taken together, these data highlight the intricate control of osteoblast homeostasis by PDE5A, with a net skeletal anabolic advantage of PDE5A inhibition exerted through enhanced mineralization and new bone formation (Figs. 3 and 4 *A* and *B*).

Discussion

We report that the two widely used drugs for erectile dysfunction, tadalafil and vardenafil, increase bone mass by coordinated peripheral and central actions. Notably, despite yielding an antiproliferative gene signature consistent with sympathetic relay, which can be traced upstream to specific brain neurons, the two drugs also exhibited a unique peripheral gene signature, with demonstrable increases in osteoblastogenesis in vitro and bone formation in vivo. In parallel, there was a reduction in osteoclastic bone resorption in vivo arising from the inhibition of osteoclastogenesis. Altogether, the anabolic action plus reduced bone removal combined to provide the robust increase in bone mass noted on DXA and replicated through μ-CT–based microstructural analyses.

Interestingly, unlike most other known osteoblast stimuli, such as parathyroid hormone or oxytocin, that trigger up-regulation of the so-called "osteoblastogenesis gene program" (45), PDE5A inhibitors modulated select genes, with *Ogn* and *Bsp* being up-regulated and *Bmp2* being suppressed. These effects could be time- or dose-dependent or both, noting that gene expression can oscillate in the sustained presence of a stimulus (46). However, despite this observed pattern in which *Runx2*, *Col1a1*, and *Alp* also remained unaltered, the net response was anabolic, suggesting that the osteoblastogenesis gene program on its own cannot serve as a sole surrogate for bone formation.

Equally intriguing is our finding that PDE5A immunoreactivity was colocalized with DBH in three brain regions: locus coeruleus, raphe pallidus, and paraventricular nucleus of the hypothalamus. Specifically, using the pseudorabies virus PRV152, we could trace sympathetic innervation from PDE5A-DBH dual-stained neurons directly to bone. PDE5A has been shown to be present in brain regions with potential functions in neurogenesis, memory, and stroke progression (26–28). Questions remain as to whether PDE5A is present in the human brain, and if so, what might be the consequences of any central actions of PDE5A inhibition in people.

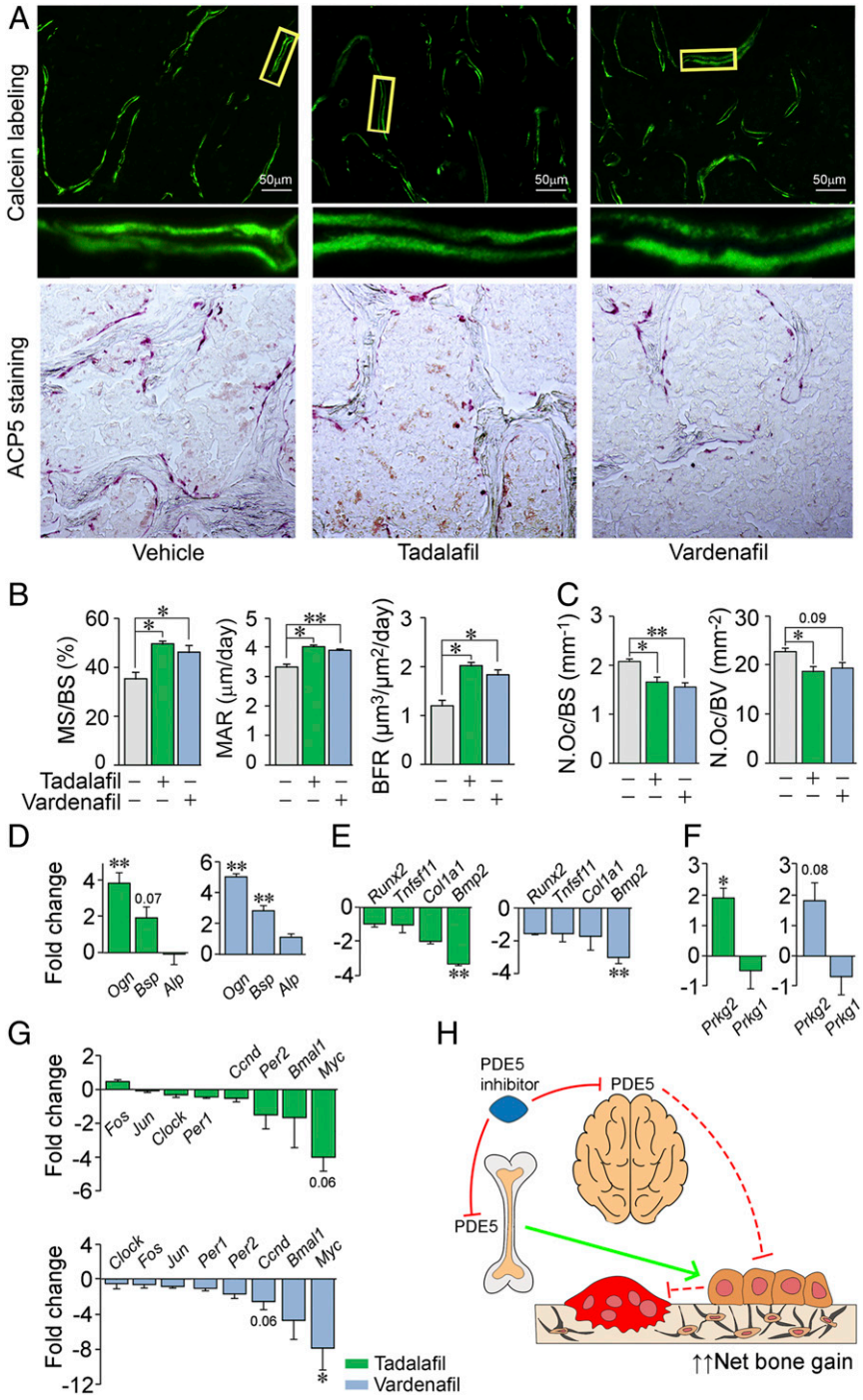

Fig. 4. PDE5A inhibitors tadalafil and vardenafil stimulate bone formation and reduce bone resorption. (*A*) Representative low-power photomicrographs (750-μm field) of calcein double labels with a magnified view (*Bottom*), as well as ACP5-stained surfaces in sections of vertebral trabecular bone at 6 wk following vehicle, tadalafil, or vardenafil treatment. (*B* and *C*) Histomorphometric analysis showing measured and calculated parameters of bone formation—MS, MAR, and BFR (5 to 24 sections from two or three mice) (*B*)—as well as number of osteoclasts (N.Oc) per bone surface (BS) or volume (BV) (9 to 20 sections from 3 to 5 mice) (*C*) (details and doses in *Methods*). Blinded measurements were made. Statistics: two-tailed Student's *t* test; $*P < 0.05$, $**P < 0.01$, or as shown vs. vehicle. Osteoblastic gene signature (SYBR Green qPCR) consisting of a set of differentially regulated differentiation genes (*Ogn*, *Bsp*, *Alp*, *Runx2*, *Tnfsf11*, *Col1a1*, and *Bmp2*) (*D* and *E*), protein kinase G isoforms (*Prkg1* and *Prkg2*) (*F*), and the unique sympathetic relay signature (39, 44) comprising *Fos*, *Jun*, *Clock*, *Per1*, *Per2*, *Bmal1*, *Ccnd*, and *Myc* (*G*), in differentiating osteoblast precursors from mice treated with tadalafil or vardenafil. (*H*) Schematic representation of the predicted roles of central and peripheral PDE5A inhibition and of reduced osteoclastic resorption in bone gain.

Erectile dysfunction is the most prevalent sexual dysfunction, affecting ∼19% of men age >20 y, with a prevalence that increases with aging (23). Furthermore, ∼47% of men age >50 y have osteopenia (34). There are also strong associations among erectile dysfunction, reduced BMD, and increased risk of hip fracture (47, 48). Thus, our data hold considerable promise for the cotherapy of erectile dysfunction and bone loss in aging men. The significantly increased *Pde5a* expression in bone in older

mice compared with young mice (Fig. 1*A*) supports this premise. In addition, when used for erectile dysfunction in androgen-deficient older men, often together with testosterone, PDE5A inhibition may, through an anabolic action, protect against the osteoporosis that is driven primarily by reduced bone formation. It is noteworthy that when administered to mildly hypogonadal men, testosterone itself does not affect bone mass or muscle strength (49).

We also posit that when used for treating erectile dysfunction in androgen-ablated prostate cancer patients, PDE5 inhibitors may prevent the acute, rapid, and severe bone loss that is poorly amenable to most other therapies (50). The drugs are also used for penile rehabilitation as a standard of care after prostatectomy (51), and this use could be extended to bone protection. In addition, and in view of the extensive safety record of PDE5A inhibitors as a class, the possibility of their repurposing for a sole use in postmenopausal women with a high fracture risk should indeed be considered. Toward this, and based on our data, we recommend safety and efficacy trials toward the utilization of all four FDA-approved agents—vardenafil, tadalafil, sildenafil, and the more recently approved avanafil—in women.

Interestingly, we found a notable discrepancy between the effective doses of vardenafil and tadalafil in mice vs. humans. Vardenafil is known to have a 10-fold higher affinity (0.89 nM) compared with tadalafil (9.4 nM) with respect to human recombinant PDE5A (22). However, in mice, tadalafil, used at a fivefold lower dose, displayed a nearly similar if not better efficacy than vardenafil. To explore this difference, we modeled mouse PDE5A using the available crystal structures of the catalytic domain of human PDE5A in combination with the respective drugs (Protein Data Bank [PDB] ID codes 1UHO for vardenafil and 1UDU for tadalafil). This allowed us to delineate subtle variations in binding modes of the respective drugs with mouse PDE5A in silico.

With a chemical structure similar to the cGMP, vardenafil binds the catalytic pocket of PDE5A and competes with cGMP binding (22, 52). In contrast, tadalafil is not related structurally to cGMP but has a similar mechanism of therapeutic action (53). Our model shows that both drugs bind mouse PDE5A and make H-bond interactions with Q807 (Fig. 5). However, the more robust actions of tadalafil on mouse bone (Figs. 3 and 4) can be explained by its greater binding energy to PDE5A (−19.4 kJ/mol) compared with vardenafil (−16.6 KJ/mol). This difference in in silico binding energy is consistent with a greater number of interactions made by tadalafil than by vardenafil (Fig. 5*C*). More importantly, the M806 residue in mouse PDE5A displays steric clashes with bound vardenafil (Fig. 5*C*), likely reducing its binding energy, and hence its potency. On a broader note, this analysis highlights the critical importance of what might appear to be relatively minimal structural variations in binding modes that could actually underpin significant potency differences in small molecules across species.

Methods

Syngeneic, 14-wk-old C57BL/6 mice, back-crossed for >10 generations, were maintained on a 12-h light/12-h dark cycle and fed on normal chow. Groups of five mice were given dimethyl sulfoxide (DMSO) (vehicle), tadalafil (2 mg/kg), or vardenafil (10 mg/kg) by oral gavage every day for 6 wk. Areal BMD was measured every 2 wk on anesthetized mice using a small animal densitometer (PIXimus). Before sacrifice at week 6, the mice were given two i.p. injections of calcein (15 mg/kg) 5 d apart and were then euthanized. Then μ-CT with three-dimensional (3D) reconstruction (μCT 40; Scanco Medical) and dynamic histomorphometry (Zeiss Axio Observer Z1) was performed, as described previously (54). For histomorphometry, images of individual sections were analyzed blinded for single- and double-labeled surface area, interlabel distance, MS, and derived bone formation calculations. Resorption surfaces were quantified blindly by TRAP staining (Sigma-Aldrich; catalog no. 387A-1KT) as described previously (54). All experimental protocols were approved by the Institutional Animal Care and Use Committee of Icahn School of Medicine at Mount Sinai.

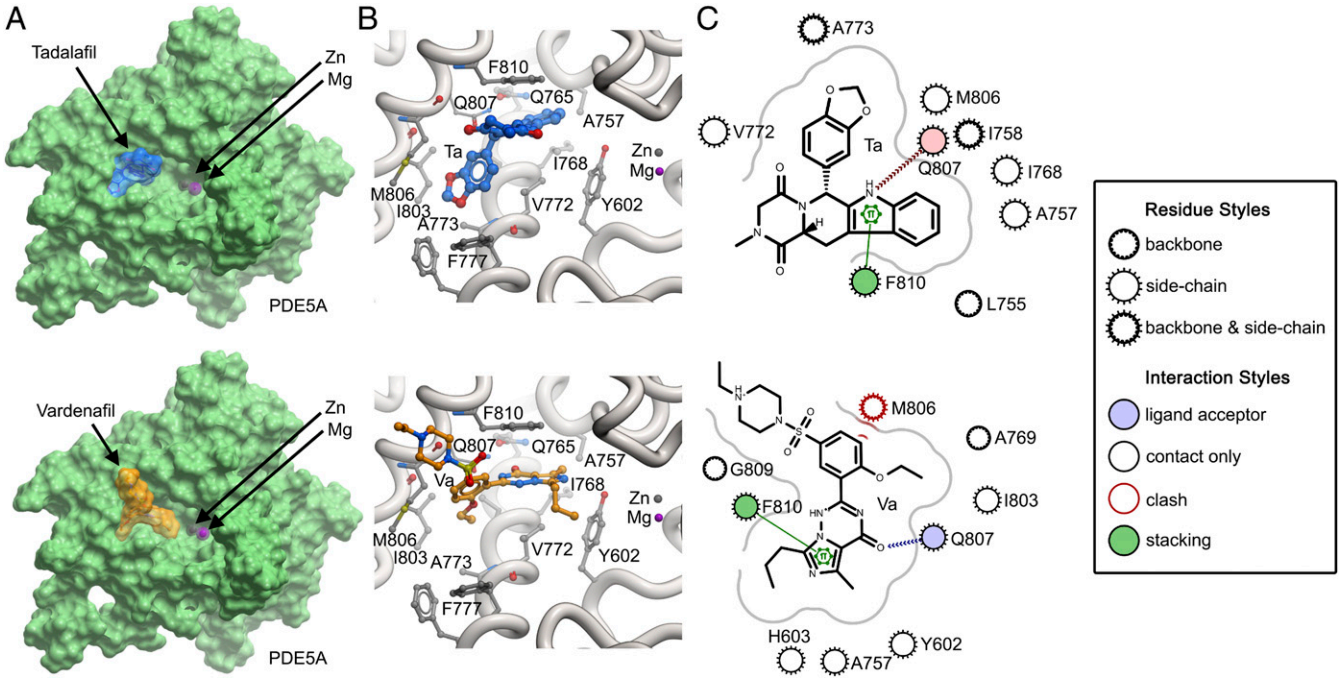

Fig. 5. Structural modeling of tadalafil and vardenafil with mouse PDE5A. (*A*) Structures of tadalafil (blue) and vardenafil (orange) positioned in the mouse PDE5A catalytic domain. The positions of Zn^{2+} (gray) and Mg^{2+} (magenta) are highlighted in the pocket. Note that catalytic activity occurs via direct interactions between cGMP and the divalent cations Zn^{2+} or Mg^{2+} (52). (*B*) Close-up of interactions by tadalafil (Ta) and vardenafil (Va) in the catalytic pocket. (*C*) Two-dimensional plot of interactions of tadalafil and vardenafil in the binding site. Note the steric clash that vardenafil makes with the side chain of M806. *SI Appendix*, Fig. S2 provides validation details.

Human CD14$^+$ cells were isolated and osteoclasts were produced in vitro using RANKL, and mineralizing osteoblasts were differentiated from human mesenchymal stem cells, as described in detail previously (55, 56). Gene screening was performed as described, using isolated RNA to make double-stranded cDNA, from which biotin-labeled cRNA was made and hybridized to the oligonucleotide DNA array on glass (57).

For immunohistochemistry, frozen marrow sections were stained with antibodies against PDE5A (rabbit polyclonal; Invitrogen, catalog no. PA5-79796), and RUNX2 (rabbit monoclonal; Abcam, catalog no. ab192256) or CSF1R (rabbit monoclonal; Invitrogen, catalog no. MA5-15151). Microwave treatment was applied after first staining to eliminate cross–reactivity as described by Toth et al. (58). Secondary antibodies included ImmPRESS-AP horse anti-rabbit IgG polymer detection kit (Vector Laboratories, catalog no. MP-5401) for PDE5A and anti-rabbit poly-HRP-IgG (Leica Biosystems, catalog no. RE7161) for RUNX2 and CSF1R. For immunolabeling frozen brain sections, we used chicken anti-GFP (Thermo Fisher Scientific, catalog no. A10262) and sheep anti-DBH (Abcam, catalog no. ab19353) as primary antibodies.

For the analysis of osteoblastogenesis, bone marrow stromal cells were grown in differentiation medium for 21 d with vehicle (DMSO), tadalafil, or vardenafil. Cells were washed, fixed and stained with alizarin red S (30 min), and photographed, after which the alizarin stain was extracted using 10% (vol/vol) acetic acid (30 min) and processed for spectrophotometry at 405 nm as described by Gregory et al. (59). Quantitative PCR assays were carried out using premade TaqMan probes (Applied Biosystems) or SYBR Green I dye for the respective genes. The data were normalized against a mixture of *Tubulin, Rps11*, *Hprt1*, *Gapdh*, and *Actb*. Data comparing groups are expressed as mean ± SEM. Comparisons used two-tailed Student's *t* tests, with a *P* value <0.05 considered significant.

For molecular modeling, we first extracted the amino acid sequence for mouse PDE5A (UniProt accession no. Q8CG03). There are two human crystal structures of the catalytic domain PDE5A in complex with vardenafil (PDB ID code 1UHO) and tadalafil (PDB ID code 1UDU) (60), with a sequence homology of 96% over 313 amino acids with the mouse sequence (*SI Appendix*, Fig. S2*A*). Residues 525 to 850 from the mouse were modeled based on the human template. The spatial positions of tadalafil and vardenafil were retained from the human structure into the mouse model. The models were built using MODELER (https://salilab.org/modeller/) and evaluated based on internal score with a stereochemical check via a Ramachandran plot (*SI Appendix*, Fig. S2*B*). Five lowest *z*-score models were selected and evaluated using ProSA (61, 62), in which a *z*-score plot and a local model quality graph were generated (*SI Appendix*, Fig. S2*C*). The *z*-score plot represents how close the quality of the MODELER program-built model is to that of the proteins of the same length generated experimentally. The energy plot shows the local energies against residue positions (*SI Appendix*, Fig. S2*D*). Since a positive value indicates errors in the modeled structure, an appropriate model should have most negative scores. Combining the results from both plots, the "best" model was then selected and was minimized to relieve any steric clashes. Figures were generated using ICM-Molsoft (63) and ezCADD (64).

Data Availability Statement. All data discussed in the paper are available in the main text and *SI Appendix*.

ACKNOWLEDGMENTS. We thank Jay Cao, PhD for his assistance with μ-CT interpretation. Support was provided by the NIH Grants (R01 AR67066, R01 DK113627, and U19 AG60917, to M.Z.; AR055208, to H.C.B.). M.I.N. is supported by the M.I.N. Children's Hormone Research Foundation.

1. I. MacIntyre *et al*., Osteoclastic inhibition: An action of nitric oxide not mediated by cyclic GMP. *Proc. Natl. Acad. Sci. U.S.A.* **88**, 2936–2940 (1991).
2. P. Collin-Osdoby, G. A. Nickols, P. Osdoby, Bone cell function, regulation, and communication: A role for nitric oxide. *J. Cell. Biochem.* **57**, 399–408 (1995).
3. P. Collin-Osdoby, L. Rothe, S. Bekker, F. Anderson, P. Osdoby, Decreased nitric oxide levels stimulate osteoclastogenesis and bone resorption both in vitro and in vivo on the chick chorioallantoic membrane in association with neoangiogenesis. *J. Bone Miner. Res.* **15**, 474–488 (2000).
4. T. P. Kasten *et al*., Potentiation of osteoclast bone-resorption activity by inhibition of nitric oxide synthase. *Proc. Natl. Acad. Sci. U.S.A.* **91**, 3569–3573 (1994).
5. B. B. Yaroslavskiy *et al*., NO-dependent osteoclast motility: Reliance on cGMP-dependent protein kinase I and VASP. *J. Cell Sci.* **118**, 5479–5487 (2005).
6. H. Zheng, X. Yu, P. Collin-Osdoby, P. Osdoby, RANKL stimulates inducible nitric-oxide synthase expression and nitric oxide production in developing osteoclasts. An autocrine negative feedback mechanism triggered by RANKL-induced interferon-beta via NF-kappaB that restrains osteoclastogenesis and bone resorption. *J. Biol. Chem.* **281**, 15809–15820 (2006).
7. S. F. Silverton *et al*., Direct microsensor measurement of nitric oxide production by the osteoclast. *Biochem. Biophys. Res. Commun.* **259**, 73–77 (1999).
8. J. Aguirre *et al*., Endothelial nitric oxide synthase gene-deficient mice demonstrate marked retardation in postnatal bone formation, reduced bone volume, and defects in osteoblast maturation and activity. *Am. J. Pathol.* **158**, 247–257 (2001).
9. C. J. Hamilton, L. S. Reid, S. A. Jamal, Organic nitrates for osteoporosis: An update. *Bonekey Rep.* **2**, 259 (2013).
10. S. Wimalawansa *et al*., Frequency-dependent effect of nitric oxide donor nitroglycerin on bone. *J. Bone Miner. Res.* **15**, 1119–1125 (2000).
11. S. J. Wimalawansa, Nitric oxide: Novel therapy for osteoporosis. *Expert Opin. Pharmacother.* **9**, 3025–3044 (2008).
12. S. J. Wimalawansa, G. De Marco, P. Gangula, C. Yallampalli, Nitric oxide donor alleviates ovariectomy-induced bone loss. *Bone* **18**, 301–304 (1996).
13. H. Kalyanaraman *et al*., A novel, direct NO donor regulates osteoblast and osteoclast functions and increases bone mass in ovariectomized mice. *J. Bone Miner. Res.* **32**, 46–59 (2017).
14. S. A. Jamal, W. S. Browner, D. C. Bauer, S. R. Cummings, Intermittent use of nitrates increases bone mineral density: The study of osteoporotic fractures. *J. Bone Miner. Res.* **13**, 1755–1759 (1998).
15. L. Rejnmark, P. Vestergaard, L. Mosekilde, Decreased fracture risk in users of organic nitrates: A nationwide case-control study. *J. Bone Miner. Res.* **21**, 1811–1817 (2006).
16. J. Abrams, The role of nitrates in coronary heart disease. *Arch. Intern. Med.* **155**, 357–364 (1995).
17. M. J. Griffiths, T. W. Evans, Inhaled nitric oxide therapy in adults. *N. Engl. J. Med.* **353**, 2683–2695 (2005).
18. G. Ramdani *et al*., cGMP-dependent protein kinase-2 regulates bone mass and prevents diabetic bone loss. *J. Endocrinol.* **238**, 203–219 (2018).
19. A. Pfeifer *et al*., Intestinal secretory defects and dwarfism in mice lacking cGMP-dependent protein kinase II. *Science* **274**, 2082–2086 (1996).
20. B. L. Homer *et al*., Oral administration of soluble guanylate cyclase agonists to rats results in osteoclastic bone resorption and remodeling with new bone formation in the appendicular and axial skeleton. *Toxicol. Pathol.* **43**, 411–423 (2015).
21. J. Joshua *et al*., Soluble guanylate cyclase as a novel treatment target for osteoporosis. *Endocrinology* **155**, 4720–4730 (2014).
22. E. Bischoff, Potency, selectivity, and consequences of nonselectivity of PDE inhibition. *Int. J. Impot. Res.* **16** (suppl. 1), S11–S14 (2004).
23. E. Selvin, A. L. Burnett, E. A. Platz, Prevalence and risk factors for erectile dysfunction in the US. *Am. J. Med.* **120**, 151–157 (2007).
24. S. H. Spencer *et al*., Erectile dysfunction medication use in veterans eligible for Medicare part D. *J. Manag. Care Spec. Pharm.* **22**, 818–824 (2016).
25. H. Barnes, Z. Brown, A. Burns, T. Williams, Phosphodiesterase 5 inhibitors for pulmonary hypertension. *Cochrane Database Syst. Rev.* **1**, CD012621 (2019).
26. A. T. Bender, J. A. Beavo, Specific localized expression of cGMP PDEs in Purkinje neurons and macrophages. *Neurochem. Int.* **45**, 853–857 (2004).
27. L. Liu *et al*., Phosphodiesterase 5 inhibitors as novel agents for the treatment of Alzheimer's disease. *Brain Res. Bull.* **153**, 223–231 (2019).
28. R. Zhang *et al*., Sildenafil (Viagra) induces neurogenesis and promotes functional recovery after stroke in rats. *Stroke* **33**, 2675–2680 (2002).
29. L. Wang, H. Jia, R. J. Tower, M. A. Levine, L. Qin, Analysis of short-term treatment with the phosphodiesterase type 5 inhibitor tadalafil on long bone development in young rats. *Am. J. Physiol. Endocrinol. Metab.* **315**, E446–E453 (2018).
30. Y. Gong *et al*., Inhibition of phosphodiesterase 5 reduces bone mass by suppression of canonical Wnt signaling. *Cell Death Dis.* **5**, e1544 (2014).
31. H. H. Alp *et al*., The effect of PDE5 inhibitors on bone and oxidative damage in ovariectomy-induced osteoporosis. *Exp. Biol. Med. (Maywood)* **242**, 1051–1061 (2017).
32. Z. Huyut, N. Bakan, S. Yıldırım, H. H. Alp, Effects of the phosphodiesterase-5 (PDE-5) inhibitors, avanafil and zaprinast, on bone remodeling and oxidative damage in a rat model of glucocorticoid-induced osteoporosis. *Med. Sci. Monit. Basic Res.* **24**, 47–58 (2018).
33. T. Histing *et al*., Sildenafil accelerates fracture healing in mice. *J. Orthop. Res.* **29**, 867–873 (2011).
34. J. M. Campion, M. J. Maricic, Osteoporosis in men. *Am. Fam. Physician* **67**, 1521–1526 (2003).
35. A. T. Bender, J. A. Beavo, Cyclic nucleotide phosphodiesterases: Molecular regulation to clinical use. *Pharmacol. Rev.* **58**, 488–520 (2006).
36. H. Dobnig, R. T. Turner, Evidence that intermittent treatment with parathyroid hormone increases bone formation in adult rats by activation of bone lining cells. *Endocrinology* **136**, 3632–3638 (1995).
37. M. Zaidi, A. M. Inzerillo, B. S. Moonga, P. J. Bevis, C. L. Huang, Forty years of calcitonin–Where are we now? A tribute to the work of Iain Macintyre, FRS. *Bone* **30**, 655–663 (2002).
38. F. Elefteriou *et al*., Leptin regulation of bone resorption by the sympathetic nervous system and CART. *Nature* **434**, 514–520 (2005).
39. S. Takeda *et al*., Leptin regulates bone formation via the sympathetic nervous system. *Cell* **111**, 305–317 (2002).
40. A. Bajayo *et al*., Skeletal parasympathetic innervation communicates central IL-1 signals regulating bone mass accrual. *Proc. Natl. Acad. Sci. U.S.A.* **109**, 15455–15460 (2012).
41. X. Zhang, X. Lv, Y. Zhang, X. Jiao, B. Chen, Propranolol prevents osteoporosis and up-regulates leptin in ovariectomized rats. *Iran. J. Pharm. Res.* **12**, 557–562 (2013).
42. R. G. Schlienger, M. E. Kraenzlin, S. S. Jick, C. R. Meier, Use of beta-blockers and risk of fractures. *J. Am. Med. Assoc.* **292**, 1326–1332 (2004).

43. B. N. Smith *et al*., Pseudorabies virus expressing enhanced green fluorescent protein: A tool for in vitro electrophysiological analysis of transsynaptically labeled neurons in identified central nervous system circuits. *Proc. Natl. Acad. Sci. U.S.A.* **97**, 9264–9269 (2000).
44. S. Takeda, G. Karsenty, Molecular bases of the sympathetic regulation of bone mass. *Bone* **42**, 837–840 (2008).
45. R. Tamma *et al*., Oxytocin is an anabolic bone hormone. *Proc. Natl. Acad. Sci. U.S.A.* **106**, 7149–7154 (2009).
46. L. Sun, G. Yang, M. Zaidi, J. Iqbal, TNF-induced gene expression oscillates in time. *Biochem. Biophys. Res. Commun.* **371**, 900–905 (2008).
47. C. H. Wu *et al*., Increased risk of osteoporosis in patients with erectile dysfunction: A nationwide population-based cohort study. *Medicine (Baltimore)* **95**, e4024 (2016).
48. C. H. Wu *et al*., Hip fracture in people with erectile dysfunction: A nationwide population-based cohort study. *PLoS One* **11**, e0153467 (2016).
49. P. J. Snyder *et al*., Effect of testosterone treatment on body composition and muscle strength in men over 65 years of age. *J. Clin. Endocrinol. Metab.* **84**, 2647–2653 (1999).
50. S. Epstein, A. M. Inzerillo, J. Caminis, M. Zaidi, Disorders associated with acute rapid and severe bone loss. *J. Bone Miner. Res.* **18**, 2083–2094 (2003).
51. Y. Nakano, H. Miyake, K. Chiba, M. Fujisawa, Impact of penile rehabilitation with low-dose vardenafil on recovery of erectile function in Japanese men following nerve-sparing radical prostatectomy. *Asian J. Androl.* **16**, 892–896 (2014).
52. J. D. Corbin, A. Beasley, M. A. Blount, S. H. Francis, Vardenafil: Structural basis for higher potency over sildenafil in inhibiting cGMP-specific phosphodiesterase-5 (PDE5). *Neurochem. Int.* **45**, 859–863 (2004).
53. M. A. Blount *et al*., Binding of tritiated sildenafil, tadalafil, or vardenafil to the phosphodiesterase-5 catalytic site displays potency, specificity, heterogeneity, and cGMP stimulation. *Mol. Pharmacol.* **66**, 144–152 (2004).
54. L. L. Zhu *et al*., Blocking antibody to the β-subunit of FSH prevents bone loss by inhibiting bone resorption and stimulating bone synthesis. *Proc. Natl. Acad. Sci. U.S.A.* **109**, 14574–14579 (2012).
55. L. Liu *et al*., Na^+/H^+ exchanger regulatory factor 1 (NHERF1) directly regulates osteogenesis. *J. Biol. Chem.* **287**, 43312–43321 (2012).
56. L. J. Robinson *et al*., Estrogen inhibits RANKL-stimulated osteoclastic differentiation of human monocytes through estrogen and RANKL-regulated interaction of estrogen receptor-alpha with BCAR1 and Traf6. *Exp. Cell Res.* **315**, 1287–1301 (2009).
57. R. Bu *et al*., Expression and function of TNF-family proteins and receptors in human osteoblasts. *Bone* **33**, 760–770 (2003).
58. Z. E. Tóth, E. Mezey, Simultaneous visualization of multiple antigens with tyramide signal amplification using antibodies from the same species. *J. Histochem. Cytochem.* **55**, 545–554 (2007).
59. C. A. Gregory, W. G. Gunn, A. Peister, D. J. Prockop, An Alizarin red-based assay of mineralization by adherent cells in culture: Comparison with cetylpyridinium chloride extraction. *Anal. Biochem.* **329**, 77–84 (2004).
60. B. J. Sung *et al*., Structure of the catalytic domain of human phosphodiesterase 5 with bound drug molecules. *Nature* **425**, 98–102 (2003).
61. M. Wiederstein, M. J. Sippl, ProSA-web: Interactive web service for the recognition of errors in three-dimensional structures of proteins. *Nucleic Acids Res.* **35**, W407–W410 (2007).
62. M. J. Sippl, Recognition of errors in three-dimensional structures of proteins. *Proteins* **17**, 355–362 (1993).
63. R. Abagyan, M. Totrov, D. Kuznetsov, ICM—A new method for protein modeling and design: Applications to docking and structure prediction from the distorted native conformation. *J. Comput. Chem.* **15**, 488–506 (1994).
64. A. Tao *et al*., ezCADD: A rapid 2D/3D visualization-enabled web modeling environment for democratizing computer-aided drug design. *J. Chem. Inf. Model.* **59**, 18–24 (2019).